Plasma Wave Turbulence Associated With an Interplanetary Shock

D. A. GURNETT

Department of Physics and Astronomy, The University of Iowa, Iowa City, Iowa 52242

F. M. NEUBAUER

Institut für Geophysik und Meteorologie der Technischen Universität Braunschweig, 33 Braunschweig, West Germany

R. SCHWENN

Max-Planck-Institut für Physik und Astrophysik, 8046 Garching, West Germany

In this paper we give a brief summary of the interplanetary shocks detected and analyzed to date from the Helios 1 and 2 spacecraft and present a detailed analysis of the plasma wave turbulence associated with one particular shock, on March 30, 1976. This event was selected because a very clearly defined burst of plasma wave turbulence occurs at the shock with otherwise quiet conditions in the solar wind upstream and downstream of the shock. The shock is an oblique shock and the upstream parameters are characterized by a low Mach number, a low beta, and an unusually large electron to ion temperature ratio. Three types of plasma waves are detected in association with this shock: (1) electron plasma oscillations, (2) electrostatic ion-acoustic or Buneman mode turbulence from about 1 to 30 kHz, and (3) whistler-mode magnetic noise. Because of the high velocity of the shock and the quiet conditions in the solar wind this event provides a particularly good determination of the scale size and characteristics of the precursor waves upstream of the shock and the electric and magnetic field turbulence in the wake behind the shock. The primary burst of electric and magnetic field noise at the shock occurs a few seconds after the jump in the magnetic field, with a broad maximum in the electric field intensities at about 3 kHz and a monotonically decreasing magnetic field spectrum below about 1 kHz. Many of the characteristics of this shock are found to be closely similar to, and are compared with, previous observations of plasma wave turbulence associated with the earth's bow shock.

1. INTRODUCTION

For many years the investigation of shocks in collisionless plasmas has received considerable attention in both laboratory and space plasmas. Upstream of the earth's magnetosphere a collisionless shock wave is known to form in the solar wind as it flows past the earth at supersonic velocities. Because this region can be readily studied by eccentric earth orbiting spacecraft substantial progress has been made in understanding and characterizing the earth's bow shock for a wide range of plasma parameters. The current state of knowledge of the earth's bow shock has recently been reviewed by *Greenstadt and Fredricks* [1978]. Within the shock transition region it has been established [*Fredricks et al.*, 1968; *Olson et al.*, 1969] that intense electric and magnetic field turbulence is generated by plasma instabilities. This plasma wave turbulence acts to heat the incoming plasma as it flows across the shock boundary and plays a role similar to collisions in an ordinary collision-dominated shock. Electric field measurements in the transition region [*Fredricks et al.*, 1968, 1970*a*, *b*] show that the electric field turbulence is closely correlated with magnetic field gradients, indicating the presence of a current-driven instability [*Wu and Fredricks*, 1972]. Detailed studies of the dependence of the turbulence amplitude on the upstream parameters have been presented by *Rodriguez and Gurnett* [1975, 1976].

Collisionless shocks similar to the earth's bow shock also occur in the interplanetary medium in response to changes induced in the solar wind flow by solar rotation and by transient events (flares) near the sun (see, for example, *Smith and Wolfe* [1976] and *Dryer et al.* [1976]). In comparison to the earth's bow shock near the subsolar point interplanetary shocks are usually weaker. Studies of these shocks can, therefore, provide information on shock characteristics for ranges of parameters which often are not observed in the earth's bow shock. Interplanetary shocks are also of interest because of their role in the acceleration of energetic charged particles in the interplanetary medium [*Sarris and Van Allen*, 1974]. Because of the infrequent occurrence of interplanetary shocks and the absence until recently of suitable instrumentation on interplanetary spacecraft the study of plasma wave turbulence associated with interplanetary shocks is in a relatively early stage of investigation. Electric field observations associated with an interplanetary shock have been reported by *Scarf et al.* [1974] and magnetic field observations have been reported by *Neubauer et al.* [1977]. For a review of these and other observations see *Scarf* [1978]. The purpose of this paper is to give a brief survey of the plasma wave turbulence observed in association with interplanetary shocks detected by the solar-orbiting Helios 1 and 2 spacecraft and to present a detailed analysis of one particular event, on March 30, 1976.

The Helios 1 and 2 spacecraft, which were launched on December 10, 1974, and January 15, 1976, are in eccentric solar orbits near the ecliptic plane with initial perihelion radial distances of 0.309 and 0.290 AU and aphelion radial distances of 0.985 and 0.983 AU, respectively. The plasma wave electric field measurements presented in this study are from the University of Iowa electric field experiment on Helios 1 and 2. This experiment uses a dipole antenna for electric field measurements and provides electric field intensities in 16 filter channels from 31.1 kHz to 178 kHz. A detailed description of this experiment is given by *Gurnett and Anderson* [1977]. The wave magnetic field measurements are from the Technical University of Braunschweig search-coil magnetometer experiment on Helios 1 and 2. This experiment is described by *Dehmel et al.* [1975] and *Neubauer et al.* [1977*a*, *b*]. Briefly the experiment

Paper number 8A0987.
0148-0227/79/008A-0987$01.00

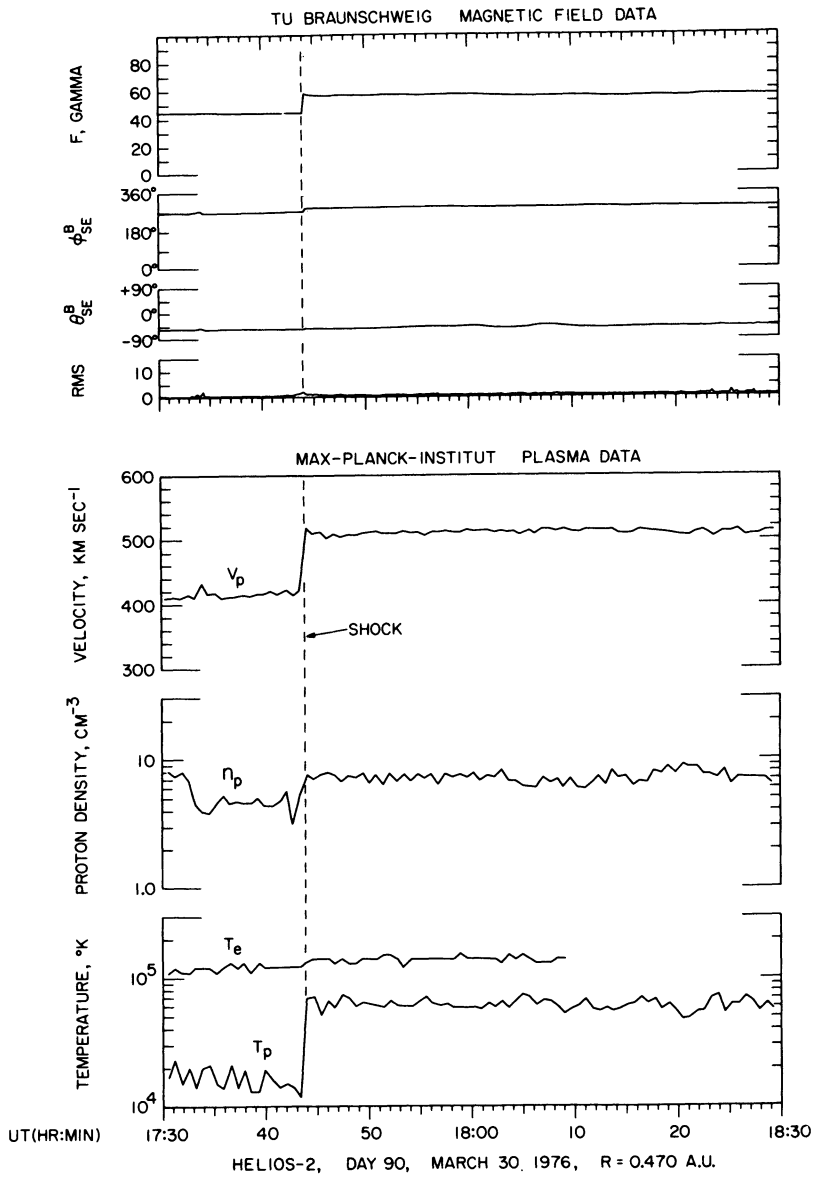

Fig. 1. The Helios 2 magnetic field and solar wind plasma data for the interplanetary shock on March 30, 1976. Note the relatively quiet conditions in the solar wind upstream and downstream of the shock..

consists of three orthogonal search-coil magnetic field sensors mounted on a boom at a distance of 4.6 m from the center of the spacecraft. Magnetic field spectral densities are determined in eight logarithmically spaced filter channels (frequency bands 4.7–10 Hz, 10–22 Hz, etc., up to 1–2.2 kHz) for each of two axes, one parallel to the spin axis and the other perpendicular to the spin axis. Both experiments provide peak as well as average spectral densities. The solar wind magnetic field measurements are from the TU Braunschweig flux-gate magnetometer described by *Musmann et al.* [1975] and *Gliem et al.* [1976]. This experiment provides measurements of three orthogonal components of the magnetic field with an accuracy of ±0.2 gamma. The solar wind plasma measurements are from the Max-Planck-Institut für Physik und Astrophysik plasma analyzer described by *Schwenn et al.* [1975]. This experiment provides a full 3-dimensional ion distribution function over the energy range from 155 eV to 15.3 keV every 40.5 seconds (for bit rates above 256 bps) and electron measurements scanning the ecliptic plane over the energy range from 0.5 eV to 1.66 keV.

2. Brief Survey of the Shocks Detected by Helios and the Event Selected for Analysis

Because of the low level of solar activity during the solar minimum period the total number of shocks available for analysis in the Helios data is quite small. For the data analyzed to date, during the primary mission of Helios 1 and 2, only 5 interplanetary shocks have been identified. All of these events have enhanced levels of magnetic turbulence at the shock boundary and in the downstream region behind the shock. The intensity of this turbulence usually decreases monotonically with increasing frequency and is detectable at frequencies up to several hundred Hz. A typical example of this magnetic turbulence is discussed by *Neubauer et al.* [1977*a*, *b*]. Although the intensity and spectrum of the magnetic field turbulence vary somewhat from event to event, the noise is always ob-

served in association with a shock at intensities substantially above the threshold of the search coil magnetometer.

In comparison to the magnetic turbulence, the electric field turbulence associated with interplanetary shocks is much more highly variable. In some cases the electric field amplitudes associated with an interplanetary shock are so small that the shock-related fields cannot be distinguished from other types of waves, such as ion-acoustic waves [*Gurnett and Frank*, 1978], which are commonly observed in the solar wind. In other cases, strong bursts of broad-band electrostatic noise, similar to the earth's bow shock, are observed in association with the shock.

Because of the limited number of events which are currently available for analysis we have not yet attempted to determine which parameters control the large variations in the plasma wave turbulence associated with interplanetary shocks. Instead, we have selected one particular event, on March 30, 1976, for analysis. This event was selected because it has a very clearly defined burst of plasma wave turbulence in both the electric and magnetic field data, and because the conditions in the solar wind upstream and downstream of the shock were relatively quiet and uncomplicated. Comparisons with other solar and geophysical observations [*Pinter*, 1977] indicate that this shock probably was associated with the type 1B solar flare at 1905 UT on March 28, 1976, and the subsequent geomagnetic SSC (indicative of an interplanetary shock) at 0255 UT on April 1, 1976. At the time the shock was detected by Helios 2 the spacecraft was near the ecliptic plane approximately 9.6° west of the earth-sun line at a radial distance of 0.470 AU from the sun.

TABLE 1. Plasma and Magnetic Field Parameters for the March 30, 1976, Shock

Upstream	Downstream
$\mathbf{B}_1 = (-0.2, -24.9, -35.6)\,\gamma$	$\mathbf{B}_2 = (10.2, -32.2, -44.5)\,\gamma$
$\mathbf{v}_1 = (-419.3, -7.9, 4.0)$ km/s	$\mathbf{v}_2 = (-507.2, -7.8, -8.9)$ km/s
$\langle(-417.4, -0.7, -1.4)$ km/s$\rangle$	
$n_{p1} = 6.8$ cm^{-3}	$n_{p2} = 8.8$ cm^{-3}
$\langle 5.6$ cm$^{-3}\rangle$	
$n_{\alpha 1} = 1.6$ cm^{-3}	$n_{\alpha 2} = 2.1$ cm^{-3}
$\langle 1.3$ cm$^{-3}\rangle$	
$T_{p1} = 15{,}000$ K	$T_{p2} = 66{,}000$ K
$T_{e1} = 105{,}000$ K	$T_{e2} = 125{,}000$ K
$T_{\alpha 1}/T_{p1} \approx 1$, $T_{e1}/T_{p1} = 7.0$	$T_{\alpha 2}/T_{p2} \approx 1$, $T_{e2}/T_{p2} \approx = 1.9$
Derived Quantities	
$\beta_1 = \sum_i n_{i1} K T_i / B_1^2/8\pi = 0.016$	$\beta_2 = 0.023$
$\alpha_1 = \sphericalangle \mathbf{B}_1, \mathbf{v}_1 = 89.6°$	$\alpha_2 = 99.2°$
$\theta_1 = \sphericalangle \mathbf{n}, \mathbf{B}_1 = 47.5°$	$\theta_2 = 58.4°$
$V_{A1} = \lvert\mathbf{B}_1\rvert/(4\pi\rho_1)^{1/2} = 259$ km/s	$V_{A2} = 294$ km/s
Mach Numbers	
$M_{A1} = \lvert\mathbf{v}_1\rvert/V_{A1} = 1.62$	$M_{A2} = 1.73$
$A_{n,1} = v_{n,1}/B_n/(4\pi\rho_1)^{1/2} = 1.80$	$A_{n,2} = 1.60$
$M_{f,1} = v_{n,1}/c_{f,1} = 1.20$	$M_{f,1} = v_{n,2}/c_{f,2} = 0.80$
Characteristic Frequencies	
$f_{cp1} = 0.67$ Hz	$f_{cp2} = 0.86$ Hz
$f_{ce1} = 1.23$ kHz	$f_{ce2} = 1.58$ kHz
$f_{pe1} = 26$ kHz	$f_{pe2} = 29.6$ kHz
$f_{pp1} = 611$ Hz	$f_{pp2} = 691$ Hz
Characteristic Length Scales	
$c/\omega_{pe1} = 1.8$ km	$c/\omega_{pe2} = 1.6$ km
$c/\omega_{pp1} = 77$ km	$c/\omega_{pp2} = 69$ km
$\lambda_{D1} = 5.52$ m	$\lambda_{D2} = 4.75$ m
Propagation Parameters	
shock speed: 627 km/s	
shock normal: $\mathbf{n} = -(0.738, 0.334, 0.586)$	

3. Macroscopic Analysis of the March 30, 1976, Shock

The magnetic field and solar wind plasma data from Helios 2 for the period of interest, from 1730 to 1830 UT, on March 30, 1976, are illustrated in Figure 1. The top four panels show the magnetic field magnitude, direction and RMS fluctuations from the flux-gate magnetometer, and the bottom three panels show the proton velocity, proton density, and electron and proton temperatures from the solar wind plasma experiment. The polar and azimuthal angles of the magnetic field direction, $\theta_{SE}{}^B$ and $\varphi_{SE}{}^B$, are given in the usual solar ecliptic coordinates. For the time interval under consideration the sampling rate for the magnetic field measurements was one vector per second. The magnetic field data shown in Figure 1 are 8 second averages. The time resolution of the plasma measurements in Figure 1 is 40.5 seconds, which is the highest resolution available.

The high time resolution magnetic fields data show that the primary jump in the magnetic field magnitude occurred in less than one second, at 1744:00.5 UT ±0.5 s. The plasma data show that the jump in the solar wind velocity occurred between 1743:52 and 1744:11 UT, which is consistent with the magnetic field measurements. On the time scale shown in Figure 1 the solar wind on both sides of the shock is extremely quiet, making this event well suited for a detailed analysis of the upstream and downstream plasma parameters. Averaging the magnetic field components over 240 seconds and the plasma parameters over seven spectrums (283.5 seconds) gives the quantities shown in Table 1. Parameters upstream and downstream of the shock are denoted by subscripts 1 and 2, respectively. Because the proton temperature in front of the shock is unusually low the plasma parameters are subject to substantial errors. This is particularly true for the proton density, n_{p1}, and the proton temperature, T_{p1}. This problem does not exist for the downstream plasma. In order to obtain optimum plasma parameters both the magnetic field vectors and the measured downstream plasma parameters have been used to compute the upstream parameters and at the same time to check the consistency of the shock parameters (speed and normal) with the MHD-Rankine-Hugoniot relations [*Jeffrey and Taniuti*, 1964]. Where a computed value is considered to be more accurate than the observed one, it is used in Table 1 with the observational value given in brackets. All upstream and downstream quantities not included in brackets are measured quantities.

Since the magnetic field changes direction quite significantly at the shock the coplanarity theorem can be used to obtain the shock normal, $\mathbf{n} = -(0.738, 0.334, 0.586)$, in solar-ecliptic ($x$, y, z) coordinates. The shock is therefore coming from the NE-quadrant of the sun as seen from the spacecraft. The angles between magnetic field and the shock normal are $\theta_1 = 47.5°$ and $\theta_2 = 58.4°$, respectively, indicating an oblique shock. Because of the unusually low density and large magnetic field strength at 0.47 AU the plasma beta is extremely small, $\beta_1 = 0.016$ and $\beta_2 = 0.023$, even behind the shock. Using β_2, θ_1 and θ_2, the expected density ratio can be computed across the shock, leading to a theoretical value of $n_{p1} = 6.8$ cm^{-3}. The experimental value $n_{p1} = 5.6$ cm^{-3} is shown in brackets and is well within the expected experimental error (~±20%) for the

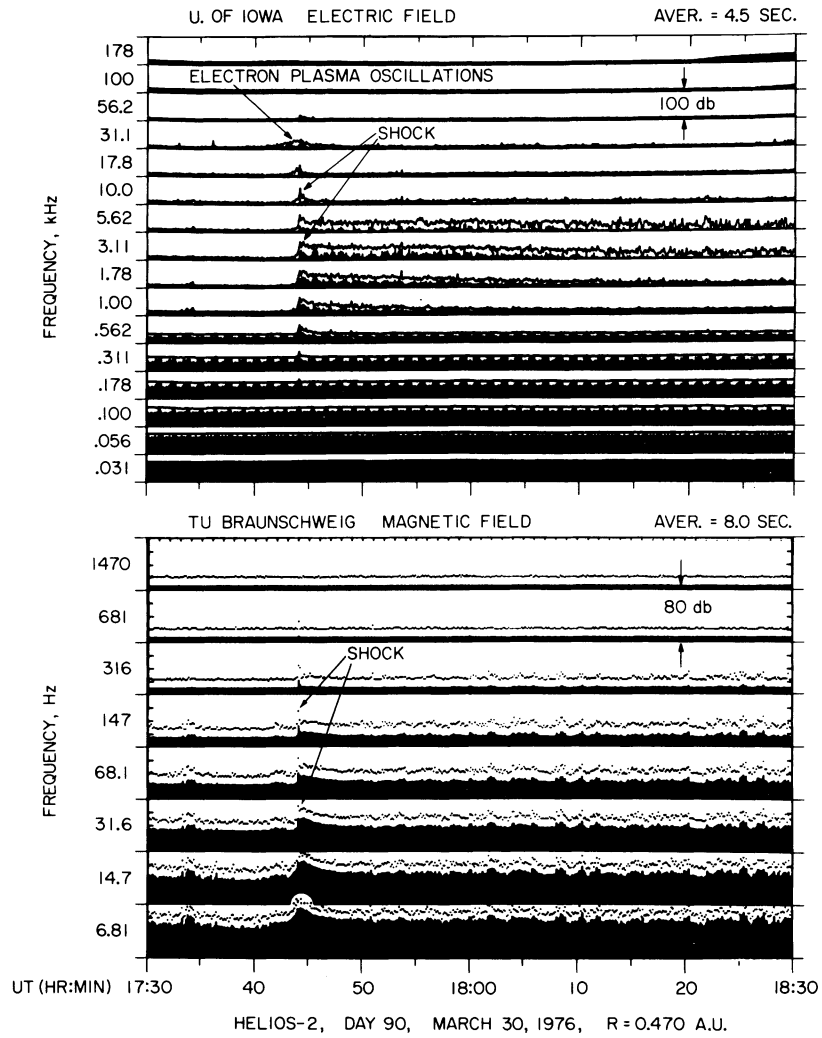

Fig. 2. The electric and magnetic field intensities associated with the shock on March 30, 1976, on a time scale corresponding to Figure 1. The shock occurred at 1744:00.5 UT ±0.5 s. Note the narrow band electron plasma oscillations upstream of the shock, the abrupt burst of noise at the shock, and the broad band of electric and magnetic field turbulence in the wake region downstream of the shock.

density determination. The shock is unusual because of the extremely large α-particle to proton ratio, $n_\alpha/n_i = 0.24$, which is the same on both sides of the shock, and the large electron to ion temperature ratio, $T_{e1}/T_{p1} = 7$, in the upstream region.

The Alfvén Mach numbers A_n computed from the normal components V_n of the velocity vectors in the shock frame and the magnetic field are $A_{n,1} = 1.8$ and $A_{n,2} = 1.6$ which are greater than one as required for a fast MHD-shock. The fast Mach numbers M_f based on the fast magnetoacoustic speed $C_f(\theta)$ turn out to be $M_{f,1} = 1.2 > 1$ and $M_{f,2} = 0.8$ respectively. The Alfvén Mach numbers M_{A1} and M_{A2}, with $M_A = |\mathbf{V}|/V_A$ where V_A is the Alfvén speed, are also given for later use. Using these parameters the Rankine-Hugoniot relations also yield an independent determination of the upstream velocity vector $\mathbf{V}_1 = (-419.3, -7.9, 4.0)$ km/s, which is in very good agreement with the observationally determined quantity in brackets. The propagation speed of the shock in the direction of the normal is 627 km/s.

4. Plasma Wave Turbulence Associated With the March 30, 1976, Shock

The plasma wave electric and magnetic field intensities associated with the March 30, 1976, shock are shown in Figure 2, on a time scale corresponding to the magnetic field and plasma data in Figure 1. The electric field intensities are given in 16 frequency channels from 31.1 Hz to 178 kHz and the z-axis magnetic field intensities are given in 8 frequency channels from 6.81 Hz to 1.47 kHz. The intensity scale is logarithmic with a range of 100 dB, from approximately 1 μV/m to 0.1 V/m, for the electric field measurements and a range of 80 dB, from 10^{-5} to 10^{-1} gamma/Hz$^{1/2}$, for the magnetic field measurements. The solid lines for the electric field measurements and the dots for the magnetic field measurements show the peak field intensity over each measurement interval and the vertical bars (solid black areas) show the average field intensities. For the period of interest the sampling rate is one complete spectrum of peak and average field intensities every 4.5 seconds. The electric field intensities in Figure 1 are plotted on 4.5 second intervals and the magnetic field intensities are plotted on 8 second intervals, after appropriate averaging of the individual data points. The rapid increase of the electric field background at low frequencies is caused by electrical interference from the spacecraft solar array [see *Gurnett and Anderson*, 1977]. The enhanced background noise level in the low frequency magnetic field channels ahead of the shock is caused by low level magnetic field fluctuations which are essen-

tially always present in the solar wind [see *Neubauer et al.*, 1977*b*].

Because interplanetary shocks can provide unique information on the large scale structure of a shock, with less uncertainty concerning the motion of the shock compared to studies of the earth's bow shock, we first concentrate on describing the large scale features of the plasma wave turbulence upstream and downstream of the March 30, 1976, shock. Upstream of the shock electrostatic electron plasma oscillations at the local electron plasma frequency (f_{pe} = 26 kHz) are clearly evident in Figure 2, starting about 5 minutes before the shock and increasing exponentially in intensity as the shock approaches. These upstream plasma oscillations are qualitatively similar to the electron plasma oscillations commonly found upstream of the earth's bow shock in association with suprathermal electrons streaming into the solar wind from the shock [*Scarf et al.*, 1977]. Using the shock velocity of 627 km/s from Table 1 it is estimated that the *e*-folding distance of the electron plasma oscillations upstream of this shock is about 1.9 × 10^5 km.

Electron plasma oscillations are also evident with somewhat reduced intensities in the downstream region behind the shock. The presence of plasma oscillations in the region behind the shock differs from the usual situation in the earth's bow shock, for which electron plasma oscillations are seldom detected downstream of the shock [*Rodriguez and Gurnett*, 1975].

In the region behind the shock both the electric and magnetic field data in Figure 2 show the occurrence of a long extended region of plasma wave turbulence. For the electric field this wake turbulence is mainly concentrated in the frequency range from 1 to 10 kHz, with maximum intensity at about 3 kHz. For the magnetic field the turbulence is mainly at frequencies below about 500 Hz, somewhat below the electron gyrofrequency, increasing rapidly in intensity with decreasing frequency. After the initial large burst at the shock both the electric and magnetic field intensities are seen to have a remarkably linear decrease in intensity with increasing time. For the semilogarithmic scale used this variation corresponds to a simple exponential decay, $e^{-|x|/L}$, where x is the distance nor-

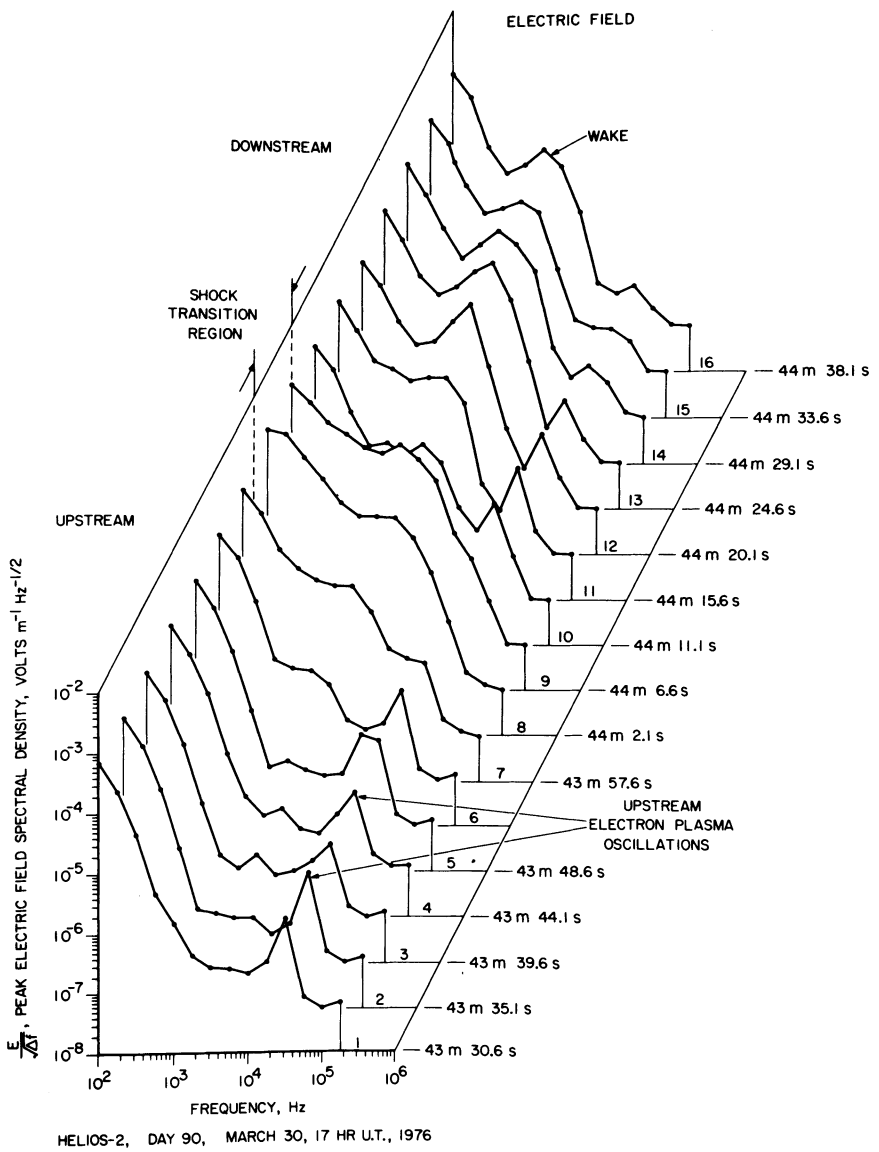

Fig. 3. A sequence of electric field spectrums through the shock transition with the highest time resolution available. Each spectrum gives the peak field intensity over the 4.5 s interval since the preceding spectrum. The jump in the magnetic field strength at the shock occurs at 44 min 0.5 s (see Figure 5).

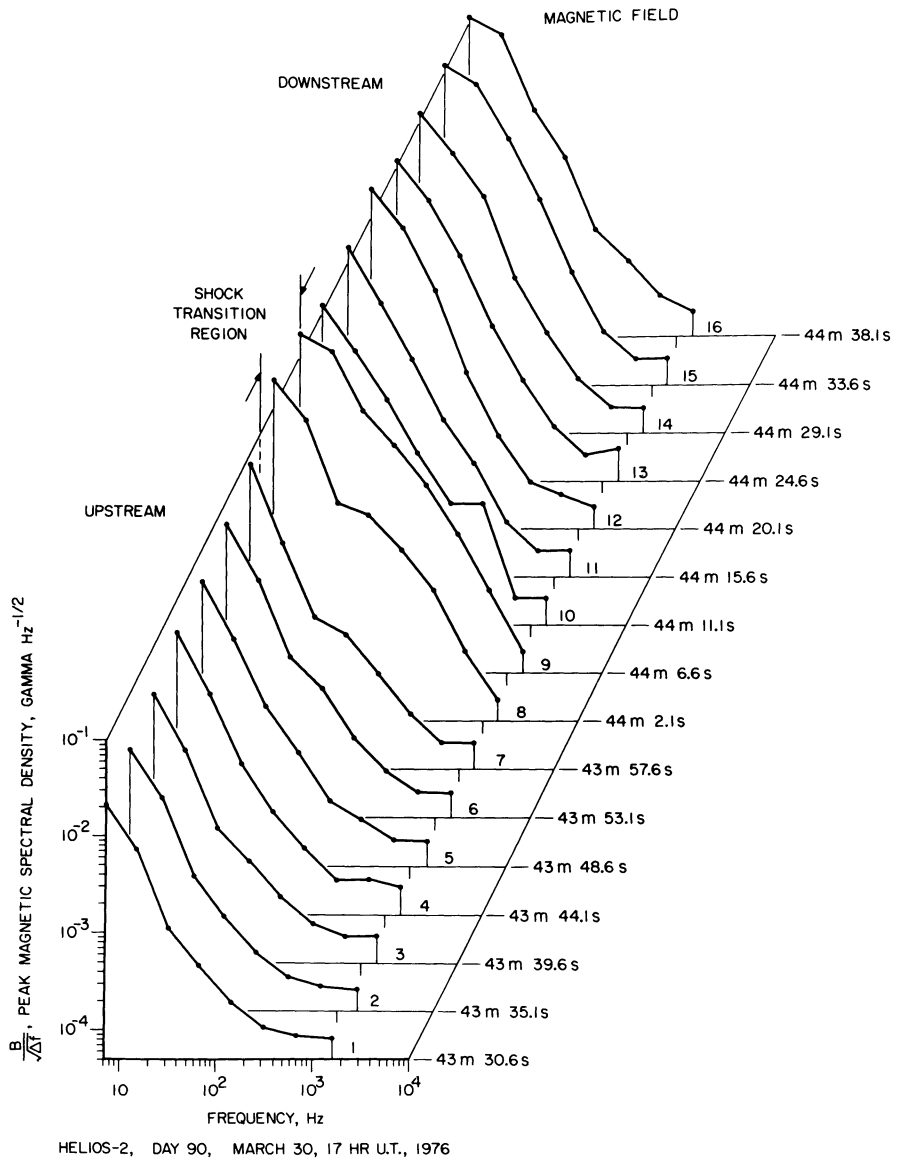

Fig. 4. A sequence of magnetic field spectrum through the shock transition on a time scale corresponding to Figure 3. The intensities are again peak values, however the times correspond to the center of each 4.5 s peak sampling interval.

mal to the shock and L is a characteristic e-folding length. For the magnetic field the e-folding length increases slightly with increasing frequency. Using the shock speed and shock normal direction from Table 1 the e-folding lengths for the magnetic field turbulence are found to vary from about $L \simeq 1.3 \times 10^5$ km at 6.81 Hz to $L \simeq 2.5 \times 10^5$ km at 147 Hz. The e-folding lengths for the electric field turbulence are significantly longer than for the magnetic field turbulence and have a distinct maximum at a frequency of about 3 to 5 kHz. The e-folding lengths for the electric field turbulence at 3.11, 5.62 and 10.0 kHz are about 3.8×10^5 km, 1.9×10^6 km, and 1.6×10^4 km, respectively.

Since the waves constituting the downstream turbulence are evidently being reabsorbed by the plasma, it is of interest to consider whether these waves provide a significant energy input into the plasma. At 1745:50 UT, shortly after the shock crossing, the normalized electric (>178 Hz) and magnetic (>4.7 Hz) field energy density ratios are approximately $E^2/(8\pi nkT) \simeq 7.7 \times 10^{-9}$ and $B^2/(8\pi nkT) \simeq 9.2 \times 10^{-6}$. These ratios show that the wave absorption provides a negligible energy input to the total plasma energy, although the waves may nonetheless play an important role in thermalizing the plasma.

Having discussed the regions upstream and downstream of the shock we now consider the plasma wave turbulence in the vicinity of the transition region. Figure 2 shows that the peak electric and magnetic field intensities near the shock are much larger than the average intensities. The large peak to average field strength ratios indicate that the turbulence in the transition region is very impulsive, consisting of one or more brief bursts with durations short compared to the sampling interval (4.5 seconds). The spectrum variations are illustrated in greater detail in Figures 3 and 4, which show a sequence of contiguous electric and magnetic field spectrums through the transition region. A corresponding plot of the magnetic field strength for the same interval is shown in Figure 5. The spectrums in Figures 3 and 4 are numbered, with the sampling times for the spectrums indicated at the top of Figure 5. The spectrum intensities are the maximum value of the square root of the power spectrum density, $(E^2/\Delta f)^{1/2}$ and $(B^2/\Delta f)^{1/2}$, for

each 4.5 second sampling interval. Because of differences in the internal timing of the experiments, the time for the electric field spectrums correspond to the end of each sampling interval, whereas the times for the magnetic field spectrums correspond to the midpoints of each sampling interval. The electric field spectrums in Figure 3 clearly show the upstream electron plasma oscillations, the intense burst of broadband electrostatic noise in the transition region and the relaxation to a nearly steady level of noise from 1 to 10 kHz in the downstream region. A few weak bursts of electron plasma oscillations are also evident in the downstream region, gradually merging into the broadband 1 to 10 kHz noise. The magnetic field spectrums in Figure 4 are less complex and show a relatively featureless monotonic frequency variation, decreasing in intensity with increasing frequency. Upstream of the shock low frequency precursor waves associated with the shock are present in the low frequency channels, increasing gradually in intensity as the shock approaches. These precursor waves are also evident at even lower frequencies in Figure 5.

In the shock transtition region the magnetic field intensities abruptly increase by a substantial factor at all frequencies up to 1 kHz, and then shift down to a relatively steady level in the downstream region. Although the primary jump in the magnetic field at the shock occurs in less than 1 second, both the electric and magnetic field data show very large turbulence levels for two successive 4.5 second intervals (spectrums 8 and 9) following the jump. Thus, the intense plasma wave turbulence associated with the shock occurs behind the magnetic field jump and extends over a region substantially thicker than the current sheet associated with the ramp in the magnetic field. This region of greatly enhanced turbulence is referred to as the 'shock transition region' in Figures 3, 4, and 5. Detailed analyses show that the most intense electric and magnetic field turbulence occurs during spectrum interval number 9, which starts 1.1 seconds after the magnetic field jump for the electric field measurements and 3.4 seconds after the jump for the magnetic field measurements. The electric and magnetic field spectrums for this interval are shown in greater detail in Figures 6 and 7, along with selected spectrums from the precursor and wake regions. The peak broadband rms electric field strengths for the shock spectrum in Figure 6, integrated from 311 Hz to 100 kHz, is 2.12 mV/m. The primary contribution to the broadband field strength occurs in the frequency range from about 2 to 5 kHz. The average magnetic field intensity for the shock spectrum in Figure 7 fits a power law, $B/(\Delta f)^{1/2} = 0.4\ f^{-1.3}$ gamma/Hz$^{1/2}$, to a good approximation over the frequency range, 4.7 Hz $\lesssim f \lesssim$ 50 Hz. At high frequencies the slope of the spectrum increases, with the power law index varying from about 1.3 at 50 Hz to about 2.5 at 500 Hz.

Further information on the nature of the magnetic field jump at the shock can be obtained from an analysis of the search-coil magnetic field data. Because of the spacecraft rotation the Z component of the magnetic field is best suited for this purpose. According to Table 1 the absolute change in the Z-component of the magnetic field is $\Delta B_z = 8.9$ gammas. As is shown in more detail by *Neubauer et al.* [1977*a*] the contribution from the frequency range 4.7 Hz to 2.2 kHz to the rms value of $\dot{B}_z = dB_z/dt$, i.e., $\langle \dot{B}_z^2 \rangle^{1/2}$, can be obtained from the average magnetic field spectrum. In this case $\langle \dot{B}_z^2 \rangle^{1/2}$ for the 4.5 second analysis interval which includes the shock is 10.9 gamma/s over the frequency range 4.7 Hz to 1.0 kHz. To obtain $\langle \dot{B}_z^2 \rangle^{1/2}$ over the frequency range 0 to 1.0 kHz the contribution from the 4 Hz bandwidth of the flux-gate magnetometer has been added to the search-coil data to give $\langle \dot{B}_z^2 \rangle^{1/2} = 16.0$ gamma/s. Considering the shock to be a ramp of duration Δt, we obtain $\Delta t = \Delta B_z/(4.5 \text{ s } \langle \dot{B}_z^2 \rangle) = 0.07$ s, using equation 4 from *Neubauer et al.* [1977*a*]. This time corresponds to a length scale of 44 km. In other words, if a ramp leading to $\Delta B_z = 8.9$ gammas occurred in less than 44 km the frequency integrated power spectral density of B_z would give the observed value. Of course, for the real case the contribution from wave fields must be added to the magnetic field spectrum produced by the ramp. The shock thickness must then be greater than 44 km. Theoretically, it is expected that the shock should have a thickness of several $c/\omega_{pp} = V_A/\omega_{cp}$, where V_A is the Alfvén speed and ω_{pp} and ω_{cp} are the proton plasma and proton cyclotron frequencies, respectively [*Galeev*, 1976]. From Table 1 the characteristic length c/ω_{pp} for this shock is estimated to be about 70 km, which is in reasonably good agreement with the shock thickness, $\gtrsim$44 km, estimated from the magnetic field data.

Although the time resolution is not adequate to determine

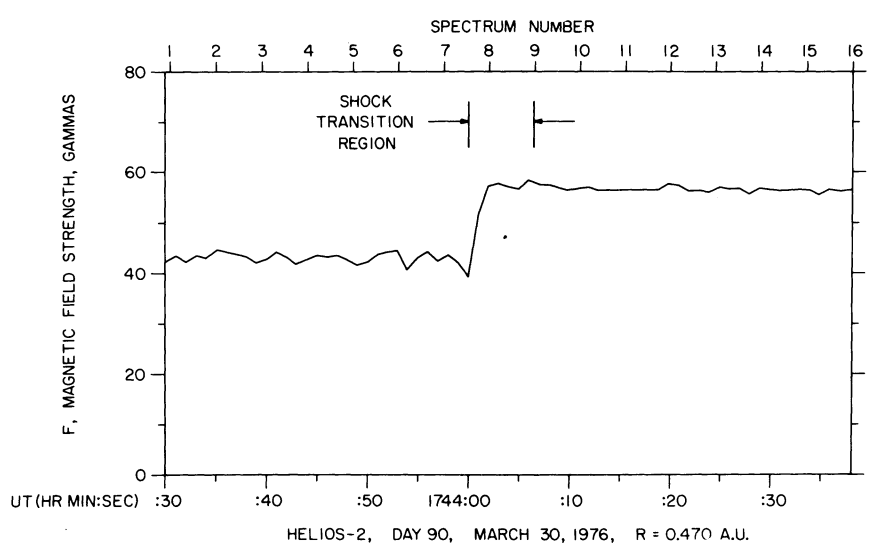

Fig. 5. The detailed magnetic field variations for the same interval as Figures 3 and 4, with the times for the corresponding spectrum numbers shown at the top. The most intense electric and magnetic field turbulence occurs in the region labeled shock transition region, a few seconds after the jump in the magnetic field.

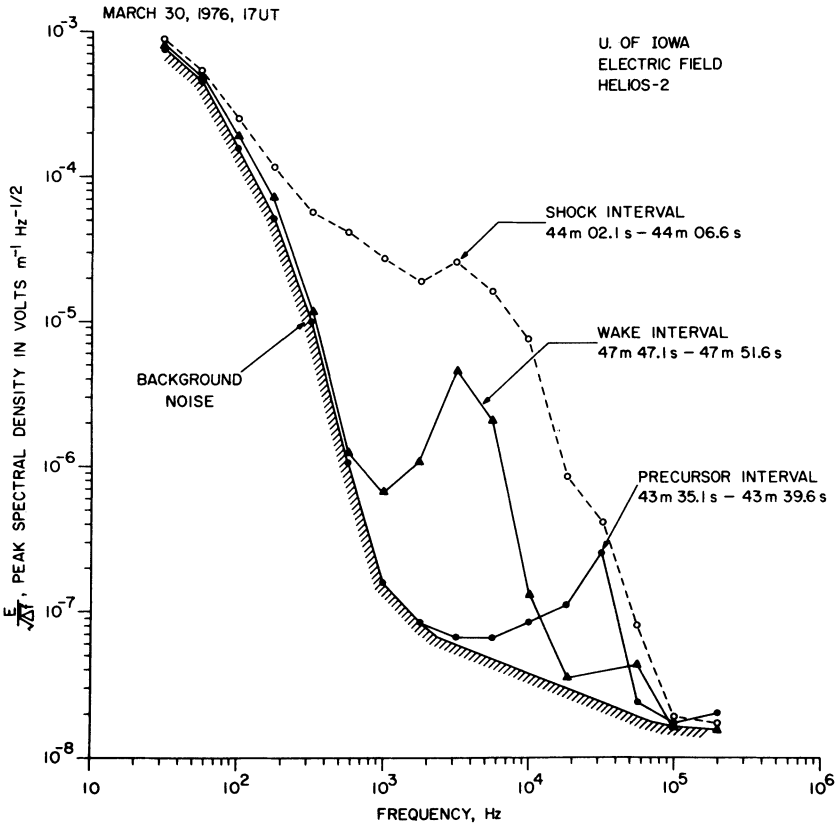

Fig. 6. Selected peak electric field spectrums in the precursor region upstream of the shock, in the transition region, and in the wake downstream of the shock. The shock spectrum (number 9 in Figure 3) corresponds to the time of maximum broadband field strength.

the polarization of the plasma wave turbulence in the transition region, some information can be obtained on the polarization of the electric fields in the wake. Figure 8 shows the angular distribution of the electric field intensities in the downstream region at 3.11 kHz, near the peak in the spectrum of the broadband electric field turbulence. This angular distribution was obtained by sorting the electric field intensities into 16 equally spaced angular sectors, based on the antenna orientation angle $\varphi_{SE}{}^{A}$ in solar ecliptic coordinates, and computing the frequency of occurrence of field intensities above fixed threshold levels. Figure 8 gives the angular variation of the electric field intensity at a constant frequency of occurrence of 20%. Since the electric field noise is very impulsive a long accumulation interval, from 1745 to 1759 UT, was necessary to reduce the statistical fluctuations to an acceptable level. The angular distribution in Figure 8 clearly shows a pronounced spin modulation, with maximum intensities at about $\varphi_{SE}{}^{A} \simeq -75°$ and $+105°$ and sharp nulls at $\varphi_{SE}{}^{A} \simeq -165°$ and $+15°$. For comparison the average direction of the magnetic field, $+\mathbf{B}$ and $-\mathbf{B}$, projected onto the ecliptic plane, $\varphi_{SE}{}^{B} \simeq -80°$ and $+100°$, are shown in Figure 8. The electric field intensities clearly have a symmetric distribution with respect to the solar wind magnetic field direction, with the maximum intensity when the antenna axis is parallel to the projected magnetic field and sharp nulls perpendicular to the magnetic field. Although the spin modulation only provides information on the electric field direction projected onto the spin plane, the sharp nulls, by about a factor of 10, together with the expected azimuthal symmetry of the electric field distribution around the magnetic field direction, provides strong evidence that the electric field of these waves is very closely aligned along the direction of the solar wind magnetic field, probably to within less than 5°. Similar results are obtained at 1.78 and 5.62 kHz.

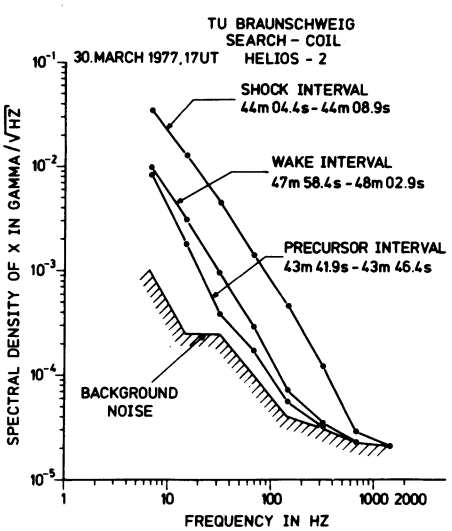

Fig. 7. Selected average magnetic field spectrums in the precursor region upstream of the shock, in the transition region, and in the wake downstream of the shock. The shock spectrum (number 9 in Figure 4) corresponds to the time of maximum broadband field strength.

5. Summary and Discussion

Because of the low level of solar activity during the solar minimum, interplanetary shocks have been relatively rare in the Helios data. Up to the present time only 5 events have been identified and analyzed. These events show a large variability

in the intensity and characteristics of the plasma wave turbulence associated with the shock, particularly for the electric fields. In some cases only very weak electric field enhancements, $\lesssim 10\ \mu$V/m, are present in association with the shock, whereas in other cases very intense bursts, $\gtrsim 1$ mV/m of electric field turbulence occurs at the shock and in the regions upstream and downstream from the shock. To illustrate the types of plasma waves which can occur in association with an interplanetary shock one particular event, on March 30, 1976, was selected for analysis. This event was selected because it displayed a very substantial and well-defined burst of electric and magnetic field noise at the shock, with usually quiet conditions in the solar wind upstream and downstream of the shock. The shock is an oblique shock ($\theta_{Bn,1} = 47.5°$) and is characterized by a low Mach number ($A_{n,1} = 1.80$, $M_{f,1} = 1.2$), a low beta ($\beta_1 = 0.016$) and an unusually large electron to ion temperature ratio ($T_{e1}/T_{p1} = 7.0$) upstream of the shock.

Three distinctly different types of plasma waves can be identified in association with this shock, (1) narrow-band electron plasma oscillations, (2) a broad band of electrostatic noise from about 1 to 30 kHz, and (3) a monotonic spectrum of low frequency magnetic noise extending up to frequencies of about 1 kHz. The observation of electron plasma oscillations in association with an interplanetary shock is apparently new and unique, since none of the other shocks detected by Helios have electron plasma oscillations and no events of this type have been previously reported. These observations of electron plasma oscillations associated with an interplanetary shock are possibly of importance to the understanding of type II and type IV solar radio bursts, since for many years it has been postulated that these radio emissions are generated by electron plasma oscillations produced by shock waves in the solar corona [*Kundu,* 1965]. In fact, the solar flare responsible for the shock analyzed is accompanied by a complex type II radio burst at frequencies from about 25 to 200 MHz, starting at 1921 UT on March 28, 1976 [*Maxwell,* 1977]. Although Helios is too far from the sun to directly detect the plasma oscillations associated with these high frequency radio emissions, the observation of electron plasma oscillations at 0.47 AU strongly suggests that similar plasma oscillations, probably with even greater intensities, are present closer to the sun. No locally generated radio emissions were detected from the plasma oscillations observed by Helios, evidently because of their low intensities, which are only about 35 μV/m.

Electron plasma oscillations, similar to the March 30, 1976, event are also commonly observed upstream of the earth's magnetosphere [*Scarf et al.,* 1971], in association with suprathermal, 100 eV to 10 keV, electrons streaming into the solar wind from the shock. It is presumed that the plasma oscillations detected by Helios are generated by essentially the same mechanism. Although it is known that the electron beams which generate plasma oscillations upstream of the earth's bow shock can propagate at least several earth radii, no definite determination has been made of the scale length over which these waves are generated. The Helios observations clearly show that the plasma oscillation intensity increases

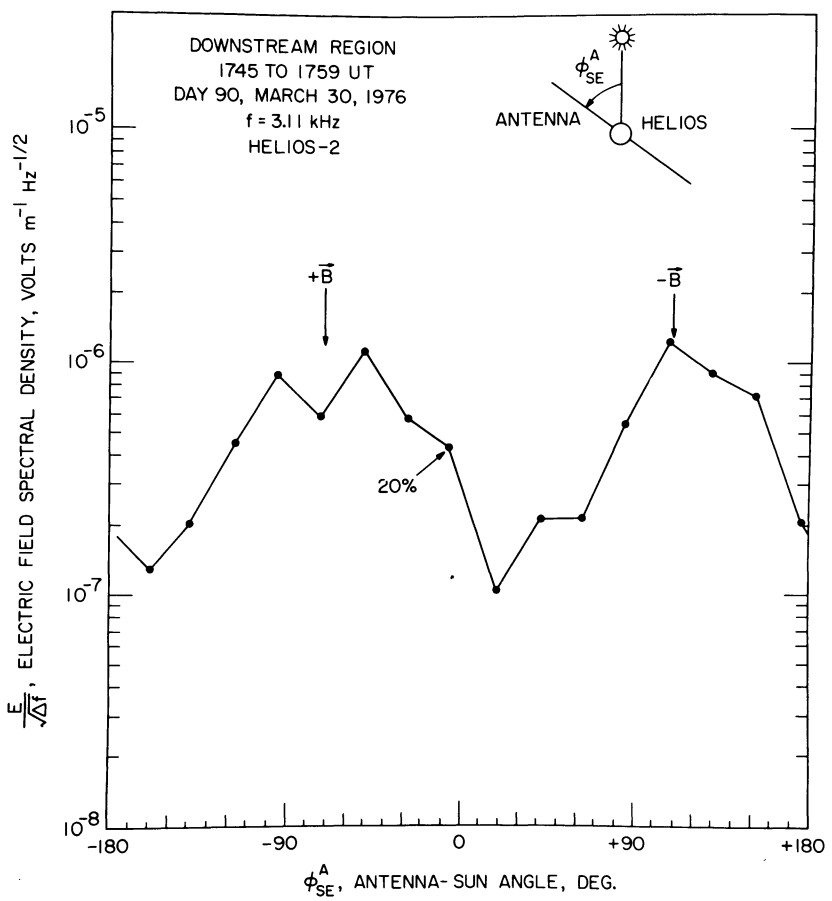

Fig. 8. The angular distribution of electric field intensities at 3.11 kHz in the wake region behind the shock. The sharp nulls when the antenna is aligned parallel to **B** and $-$**B** indicates that the electric field turbulence in the wake is aligned very closely along the direction of the solar wind magnetic field.

exponentially with decreasing distance from the shock. The *e*-folding distance is found to be about 190,000 km, which is consistent with our current knowledge of plasma oscillations associated with the earth's bow shock. This scale length presumably represents the combined effects of the growth rate of the plasma oscillation and the attenuation of the electron beam by wave-particle interactions as the beam propagates into the undisturbed plasma ahead of the shock.

Detailed comparisons of the transition region electric field spectrum in Figure 6 with spectrums given by *Rodriguez and Gurnett* [1975, 1976] from the earth's bow shock show a very close similarity. Of particular interest is the broad peak in the spectrum at about 3 kHz, which is a characteristic feature of the electric field spectrums in the earth's bow shock, although usually at somewhat lower frequencies, typically from 200 to 800 Hz. A comparable broad peak is also evident in the spectrum of the September 15, 1974, interplanetary shock investigated by *Scarf* [1978]. The unusually large electric field intensities for the shock analyzed in this paper, compared to the other events detected by Helios, also appear to be consistent with the correlations found by *Rodriguez and Gurnett* [1976], which show that large electric field intensities tend to be associated with large electron to ion temperature ratios, T_{e1}/T_{p1}, upstream of the shock. As mentioned earlier, T_{e1}/T_{p1} was unusually large for the shock analyzed. Because of the possibility of large Doppler shifts and the unknown wave number distribution in the transition region the exact identification of the waves modes responsible for the transition region electric field turbulence remains difficult. In accordance with the discussion of *Greenstadt and Fredricks* [1978] the most likely plasma wave mode responsible for this turbulence is the ion-acoustic mode, although other possibilities such as the Buneman mode [*Buneman,* 1958] cannot be completed ruled out.

The broad band of electrostatic turbulence from 1 to 10 kHz observed by Helios downstream of the transition region has features broadly similar to the electrostatic turbulence in the magnetosheath, downstream of the earth's bow shock. As described by *Rodriguez and Gurnett* [1975], the magnetosheath electrostatic turbulence has a spectrum similar to the transition region, with a broad peak at a few kHz and intensities about 1 to 2 orders of magnitude smaller than the transition region. The electric field of the magnetosheath electrostatic turbulence is also aligned parallel to the magnetic field [*Rodriguez,* 1979], in agreement with the electric field polarization determined from Helios (see Figure 8) downstream of the shock. Because of the high velocity of the shock relative to the spacecraft the Helios observations provide a determination of the large scale structure of the wake region which cannot be easily obtained from studies of the earth's bow shock. Most remarkable is the very nearly exponential decay of the electric field intensities in the wake and the occurrence of a distinct peak in the spectrum at about 3 to 5 kHz. The exponential decay and the emergence of a characteristic frequency strongly suggests that this turbulence consists of a weakly damped electrostatic mode excited by the shock which is slowly decaying in amplitude as the plasma carries the waves downstream of the shock. The impulsive variations indicated by the large ratio of peak to average field strengths (see Figure 2) suggests that these waves occur in small isolated packets or clumps which are encountered by the spacecraft on a more or less random basis.

When considering the possible plasma wave modes which could account for these waves two possibilities naturally come to mind, the ion-acoustic mode and the Buneman mode [*Buneman,* 1958]. Since ion-acoustic waves are thought to play an important role in the transition region [*Greenstadt and Fredricks,* 1978], it is reasonable to propose that the wake turbulence simply consists of slowly decaying ion-acoustic waves. Since the ion-acoustic mode can only propagate at frequencies below the ion plasma frequency, f_{pp}, which from Table 1 is only about 691 Hz, very large Doppler shifts are required to explain the observed frequency spectrum, which has a distinct peak at about 3.11 kHz (see Figure 6). Fortunately, a reasonably accurate estimate of the Doppler shift can be made in this case. The Doppler shift is given by

$$\Delta f = \frac{V}{\lambda} \cos \theta_{kV}$$

where V is the solar wind velocity, λ is the wavelength, and θ_{kV} is the angle between the solar wind velocity and the wave vector $\mathbf{k}$. Since the wake electric field turbulence is purely electrostatic the wave vector direction is parallel to the electric field. As shown earlier the electric field of this noise is very nearly parallel to the magnetic field. Therefore, θ_{kV} is approximately equal to the angle between the magnetic field and the solar wind velocity, which from Table 1 gives $\theta_{kV} \simeq \alpha_2 = 99.2°$. To compute the Doppler shift an assumption must be made concerning the wavelength of the ion-acoustic waves. For wave frequencies approaching the ion plasma frequency, the wavelength of the ion-acoustic mode approaches the minimum wavelength for waves in a plasma, which is given approximately by $\lambda_{\min} = 2\pi\lambda_D$, where λ_D is the Debye length [*Stix,* 1962]. Using $\lambda_{D2} = 4.75$ m, $V_2 = 507.2$ km/s and $\theta_{kV} = 99.2°$ the corresponding Doppler shift is $\Delta f = -2.72$ kHz. The frequency in the spacecraft frame of reference would be $f' \simeq |f_p + \Delta f| = 2.03$ kHz. As can be seen from Figure 6 this frequency is in reasonably good agreement with the frequency of maximum intensity (3.11 kHz) of the wake turbulence. Thus, the wake electric field turbulence can be accounted for by ion-acoustic waves which have wavelengths very close to the minimum wavelength, $k\lambda_D \sim 1$. One difficulty with this interpretation is that significant wave intensities are still observed at frequencies as high as 10 kHz (see Figure 6), which would imply wavelengths somewhat shorter than the minimum wavelength $2\pi\lambda_D$. This difficulty also occurs for ion-acoustic waves in the transition region, since the electric field spectrum in this region has significant intensities up to frequencies as high as 56 kHz, which is too high to be accounted for by the maximum possible Doppler shift, even if we let $\theta_{kV} = 0°$. *Scarf* [1978] has noted a similar problem in his analysis of the September 15, 1974, event. Although troublesome, this difficulty is probably not serious since the wavelengths would only have to be smaller than the minimum wavelength by a modest factor and the minimum wavelength condition is only an approximate limit caused by the onset of strong Landau damping as $k\lambda_D \to 1$. Also the Debye length in Table 1 is somewhat uncertain because of the non-Maxwellian component of the solar wind electron distribution.

It is also of interest to consider the interpretation of the wake electric field turbulence in terms of the Buneman mode [*Buneman,* 1958]. For the Buneman mode the phase velocity is much larger than the solar wind velocity, so Doppler effects are unimportant. The characteristic frequency of the Buneman mode is $f_B = (m_e/m_p)^{1/3} f_{pe}$, which for the parameters given in Table 1 is approximately $f_B = 2.40$ kHz in the downstream region. This frequency is also seen to be in good agreement

with the frequency of maximum electric field intensity in the wake region (see Figure 6). Since the Buneman mode is a very rapidly growing instability, with growth rates comparable to the frequency, the frequency spectrum of the waves produced by this instability is expected to be very broad and impulsive, possibly comparable to the observed spectrum. The Buneman mode, however, has the difficulty that very large currents (electron-ion drift velocities comparable to the electron thermal speed) are needed to drive this instability. Since neither the plasma measurements nor the magnetic field measurements give any indication of such large currents in the relatively quiescent wake region, it is difficult to see how the Buneman mode could be driven unstable in this region, or why the resulting electric fields should display the exponential decay clearly evident in Figure 2. In the absence of any satisfactory explanation for the generation of the Buneman mode in the wake, we believe that short wavelength ion-acoustic waves provide the most satisfactory explanation of the electric field turbulence downstream of this shock.

In constrast to the uncertainty concerning plasma wave mode responsible for the electric field turbulence, the magnetic field turbulence near the shock must be propagating in the whistler mode since no other electromagnetic mode of propagation exists at frequencies between the electron and ion cyclotron frequencies. The interpretation of the magnetic field turbulence for this event is greatly simplified because of the unusually low Doppler shifts for most parts of the electromagnetic waves spectrum. The low Doppler shifts in this case are due firstly to the relatively small values of the Alfvén Mach numbers ($M_{A1} = 1.62$ and $M_{A2} = 1.73$) and secondly to the fact that the magnetic field is aligned very nearly perpendicular to the solar wind velocity ($\alpha_1 = 89.6°$ and $\alpha_2 = 99.2°$). For example, a wave propagating with a phase speed equal to the Alfvén speed along the magnetic field will undergo fractional Doppler shifts of only +1% and +28% upstream and downstream of the shock, respectively. Since for the R-mode [*Stix*, 1962] the phase speed is greater than the Alfvén speed except near the electron cyclotron frequency, f_{ce}, Doppler shifts are generally negligible for parallel propagation. For other propagation directions the Doppler shifts are still reasonably small except near resonances. Hence, the magnetic field spectrums in Figure 7 may be interpreted as lying close to the frequencies in the shock rest frame. Since the electron cyclotron frequencies range from about 1.23 to 1.58 kHz, it can be seen from Figure 7 that the magnetic field noise extends with appreciable intensities up to about $f_{ce}/2$ in the shock transition region. The approximately exponential decrease in the low frequency, $\lesssim 10$ Hz, magnetic field intensities in either direction from the shock suggests that whistler-mode turbulence generated in the shock can propagate freely away from the shock and is gradually absorbed by cyclotron damping in the upstream and downstream regions. Measurements of the e-folding lengths for this damping give a scale length for the cyclotron damping of a few hundred thousand km. At higher frequencies, ≥ 10 Hz, most of whistler-mode radiation tends to be directed into the downstream region.

In this paper we have attempted to present a detailed analysis of one particular event for which a substantial level of plasma wave turbulence was present. It is clear from our initial investigations that the details of the plasma wave turbulence associated with a shock vary considerably from event to event. This case should therefore not be regarded as necessarily typical of all interplanetary shocks. In the future, after more events have been detected and analyzed, we plan to present a more detailed study of the range of variability of the turbulence associated with interplanetary shocks and to try to provide a better determination of the parameters which cause this variability.

Acknowledgments. The research at the University of Iowa was supported by NASA under contract NAS5-11279 and grant NGL-16-001-043. The research at the TU Braunschweig and MPI Garching was supported by the German Bundesministerium für Forschung und Technologie.

The Editor thanks E. J. Smith and R. W. Fredricks for their assistance in evaluating this paper.

REFERENCES

Buneman, O., Instability, turbulence and conductivity in a current carrying plasma, *Phys. Rev. Lett., 1,* 8, 1958.

Dehmel, G., F. M. Neubauer, D. Lukoschus, J. Wawretzko, and E. Lammers, Das Induktionsspulen-Magnetometer-Experiment (E4), *Raumfahrtforschung, 19,* 241, 1975.

Dryer, M., A. Eviatar, A. Frohlich, A. Jacobs, J. H. Joseph, and E. J. Weber, Interplanetary shock waves and comet brightness fluctuations during June–August 1972, *J. Geophys. Res., 80,* 2001, 1975.

Fredricks, R. W., C. F. Kennel, F. L. Scarf, G. M. Crook, and I. M. Green, Detection of electric-field turbulence in the earth's bow shock, *Phys. Rev. Lett., 21,* 1761, 1968.

Fredricks, R. W., F. V. Coroniti, C. F. Kennel, and F. L. Scarf, Fast time-resolved spectra of electrostatic turbulence in the earth's bow shock, *Phys. Rev. Lett., 24,* 994, 1970*a*.

Fredricks, R. W., G. M. Crook, C. F. Kennel, I. M. Green, and F. L. Scarf, Ogo 5 observations of electrostatic turbulence in bow shock magnetic structures, *J. Geophys. Res., 75,* 3751, 1970*b*.

Galeev, A. A., Collisionless shocks, in *Physics of Solar Planetary Environments,* vol. 1, edited by D. J. Williams, p. 464, AGU, Washington, D. C., 1976.

Gliem, F., G. Dehmel, G. Musmann, C. Türke, U. Krupstedt, and R. P. Kugel, Die Bordrechner der Helios-Magnetometer-Experimente E2 and E4, *Raumfahrtforschung, 20,* 16, 1976.

Greenstadt, E. W., and R. W. Fredricks, Shock systems in collisionless plasmas, in *Solar System Plasma Physics: A Twentieth Anniversary Overview,* North-Holland, Amsterdam, in press, 1978.

Gurnett, D. A., and R. R. Anderson, Plasma wave electric fields in the solar wind: Initital results from Helios 1, *J. Geophys. Res., 82,* 632, 1977.

Gurnett, D. A., and L. A. Frank, Ion acoustic waves in the solar wind, *J. Geophys. Res., 83,* 58, 1978.

Jeffrey, A., and T. Taniuti, *Non-Linear Wave Propagation,* Academic, New York, 1964.

Kundu, M. R., *Solar Radio Astronomy,* Interscience, New York, 1965.

Maxwell, A., Solar radio burst of spectral type II recorded at Fort Davis, Texas, during the period 20 March–2 May 1976, in *Collected Data Reports for STIP Interval II, Rep UAG-61,* edited by H. E. Coffey and J. A. McKinnon, p. 97, National Oceanic and Atmospheric Administration, Boulder, Colo., 1977.

Musmann, G., F. M. Neubauer, A. Maier, and E. Lammers, Das Förstersonden-Magnetofeldexperiment (E2), *Raumfahrtforschung, 12,* 232, 1975.

Neubauer, F. M., H. J. Beinroth, R. Barnstorf, and G. Dehmel, Initial results from the Helios-1 search-coil magnetometer experiment, *J. Geophys., 42,* 599, 1977*a*.

Neubauer, F. M., G. Musmann, and G. Dehmel, Fast magnetic fluctuations in the solar wind: Helios 1, *J. Geophys. Res., 82,* 3201, 1977*b*.

Olson, J. V., R. E. Holzer, and E. J. Smith, High-frequency magnetic fluctuations associated with the earth's bow shock, *J. Geophys. Res., 74,* 4601, 1969.

Pinter, S., Velocities of propagation of March/April 1976 coronal and interplanetary shock waves, in *Collected Data Reports for STIP Interval II, Rep. UAG-61,* edited by H. E. Coffey and J. A. McKinnon, p. 127, National Oceanic and Atmospheric Administration, Boulder, Colo., 1977.

Rodriguez, P., Magnetosheath electrostatic turbulence, *J. Geophys. Res.,* in press, 1978.

Rodriguez, P., and D. A. Gurnett, Electrostatic and electromagnetic turbulence associated with the earth's bow shock, *J. Geophys. Res., 80,* 19, 1975.

Rodriguez, P., and D. A. Gurnett, Correlation of bow shock plasma

wave turbulence with solar wind parameters, *J. Geophys. Res., 81,* 2871, 1976.

Sarris, E. T., and J. A. Van Allen, Effects of interplanetary shock waves on energetic charged particles, *J. Geophys. Res., 79,* 4157, 1974.

Scarf, F. L., Wave-particle interaction phenomena associated with shocks in the solar wind, in *Proceedings of the De Feiter Memorial Symposium on the Study of Traveling Interplanetary Phenomena,* D. Reidel, Hingham, Mass., in press, 1978.

Scarf, F. L., R. W. Fredricks, L. A. Frank, and M. Neugebauer, Nonthermal electrons and high-frequency waves in the upstream solar wind, 1, Observations, *J. Geophys. Res., 76,* 5162, 1971.

Scarf, F. L., R. W. Fredricks, I. M. Green, and G. M. Crook, Observations of interplanetary plasma waves, spacecraft noise, and sheath phenomena on Imp 7, *J. Geophys. Res., 79,* 73, 1974.

Schwenn, R., H. Rosenbauer, and H. Miggenrieder, Das Plasma-experiment auf Helios (E1), *Raumfahrtforschung, 19,* 226, 1975.

Smith, E. J., and J. H. Wolfe, Observations of interactions regions and corotating shocks between one and five AU: Pioneers 10 and 11, *Geophys. Res. Lett., 3,* 137, 1976.

Stix, T. H., *The Theory of Plasma Waves,* McGraw-Hill, New York, 1962.

Wu, C. S., and R. W. Fredricks, Cyclotron drift instability in the bow shock, *J. Geophys. Res., 77,* 5585, 1972.

(Received March 23, 1978;
revised September 9, 1978;
accepted September 13, 1978.)